

Regime transition from premixed to flameless oxidation in turbulent JP-10 flames

K.H.H. Goh, P. Geipel¹, F. Hampp, R.P. Lindstedt^{*}

Department of Mechanical Engineering, Imperial College, Exhibition Road, London SW7 2AZ, UK

Available online 20 September 2012

Abstract

An opposed jet configuration featuring fractal generated turbulence was used to characterise premixed fuel lean JP-10 flames with equivalence ratios (ϕ) from 0.20 to 0.80 stabilised against combustion products with a temperature of 1720 K. The cold flow turbulent Reynolds (Re_t) number was set to 122 and the estimated Damköhler (Da) numbers varied from below 0.3 ($\phi = 0.20$) to 6 ($\phi = 0.80$) with laminar flame parameters obtained from computations of the corresponding opposed jet configuration. The gradual transition from a turbulent flame to a supported burning mode related to the Homogeneous Charge Diffusion Ignition (HCDI) flameless oxidation regime was detected with features typical of conventional flames gradually disappearing for $\phi < 0.60$. A second mode transition to the corrugated flamelet regime at $\phi = 0.80$ is shown to coincide with a gradual change from gradient to counter-gradient turbulent transport. A density segregation based technique was applied to Particle Image Velocimetry (PIV) images to detect the instantaneous location of reaction zones and to provide conditional and unconditional statistics to illustrate the combustion regime transitions. Flame surface area characteristics and turbulent burning velocities were also derived to further characterise the burning modes.

© 2012 The Combustion Institute. Published by Elsevier Inc. All rights reserved.

Keywords: Opposed jets; Fractal grids; PIV; Flameless oxidation; JP-10

1. Introduction

Weinberg [1] and Hardesty and Weinberg [2] suggested the introduction of heat exchangers that use combustion products to preheat reactants and introduced the term Excess Enthalpy Combustion (EEC). The result is an increase in the overall efficiency and combustion chamber temperatures could be decreased without flame extinction

leading to a reduction in the formation of oxides of nitrogen. High temperature air combustion (HiTAC), using the concept of exhaust gas recirculation (EGR), was subsequently characterised by Katsuki and Hasegawa [3] and the term flameless oxidation introduced by Plessing et al. [4] and Wünning and Wünning [5]. Cavaliere and de Joannon [6] summarised progress in combustion technologies in terms of reaction stabilisation via preheating. Dally et al. [7,8] investigated the characteristics of Moderate and Intense Low Oxygen Dilution (MILD) combustion in a laboratory scale furnace as well as in a hot coflow burner. Mastorakos et al. [9] used the counterflow geometry to stabilise ultra lean premixed methane flames against hot combustion products in the opposing

^{*} Corresponding author. Fax: +44 20 7594 5696.

E-mail address: p.lindstedt@imperial.ac.uk (R.P. Lindstedt).

¹ Current address: Siemens Industrial Turbomachinery AB, SE-612 83 Finspong, Sweden.

stream. It was found that when the temperature of the hot product stream exceeded 1550 K, extinction was not observed even at an equivalence ratio of 0.20. Furthermore, the residual oxygen mole fraction in the hot products was found to have no significant impact on flame stabilisation. Geipel et al. [10] used a counterflow configuration [11] to further characterise the stability of lean premixed methane flames burning against hot combustion products at temperatures between 1520 K and 1820 K. The related Homogeneous Charge Diffusion Ignition (HCDI) regime was identified computationally by de Joannon et al. [12] using a laminar opposed jet configuration. The HCDI regime is of relevance to lean premixed pre-vapourized (LPP) Gas Turbine applications [12] and of particular interest under ultra-lean conditions where flame stability issues come to the fore [13]. The current work quantifies the combustion mode transition from a propagating premixed turbulent flame to a HCDI related flameless oxidation regime through the application of Particle Image Velocimetry (PIV), a density segregation technique [14] and the OH-LIF technique of Kerl et al. [15]. The study expands upon past work by providing (i) flow field statistics, (ii) conditional statistics, (iii) scalar fluxes and (iv) novel data on flames burning JP-10. (v) The influence of turbulence on the combustion regimes is analysed using a Damköhler number (Da) based approach [16].

2. Experimental techniques

The burner layout was similar to that used by Geyer et al. [17] and Böhm et al. [18] with two significant modifications as shown in Fig. 1. Firstly, the lower nozzle was fitted with a perforated plate (hole size = 4 mm; blockage ratio (BR) = 45%) used to stabilise lean ($\phi = 0.75$) premixed CH₄ flames 50 mm upstream of the nozzle exit in order to generate hot combustion products. Secondly, the upper nozzle was fitted with the fractal grid [19–21] previously used by Geipel et al. [11] in a parametric study of turbulence generation in isothermal flows. The optimal fractal grid [11] had a BR of 65% with maximum and minimum bar widths of 2 mm and 0.5 mm as shown in Fig. 2 along with the conventional grid used in the lower nozzle. The nozzle separation was set to one nozzle diameter D (=30 mm). The flames stabilised on the grid in the lower nozzle featured a bulk velocity (U_b) of 1 m/s (at 298 K) resulting in $\approx 5\%$ oxygen by volume remaining in the products according to laminar flame calculations [22]. Temperatures at the lower nozzle exit (T_b) were measured at 1720 K using a type R thermocouple connected to an Omega HH806AU unit indicating heat losses around 6% to the burner assembly. Mixtures of JP-10 (b.p. 460 K at 1 atm [23]) and air were intro-

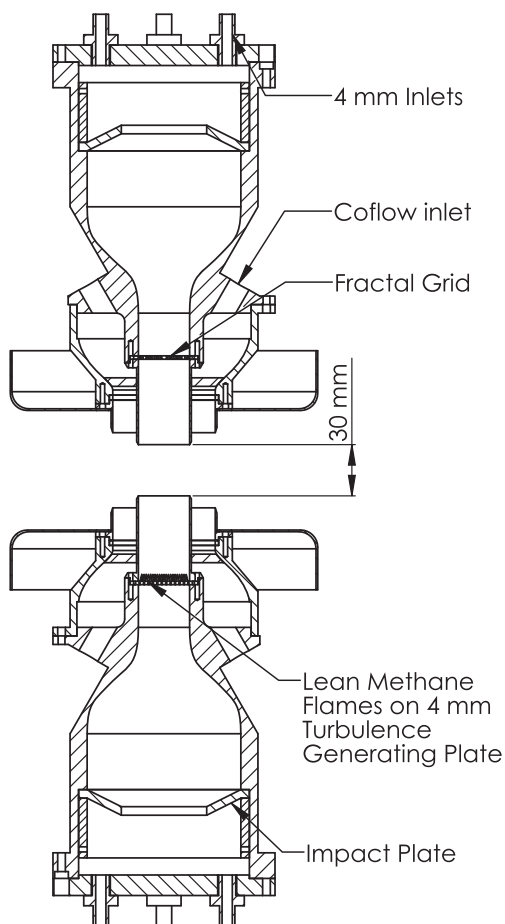


Fig. 1. Experimental configuration. JP-10/air mixtures introduced in the upper nozzle and hot products from a CH₄/air flame ($\phi = 0.75$) in the lower nozzle.

duced in the upper nozzle at $\phi = 0.20, 0.40, 0.60$ and 0.80 at $U_b = 3.5$ m/s (at 298 K) with dry air used as a reference. The integral length scale of turbulence ($L_I = 3.1 \pm 0.1$ mm) was determined by Geipel et al. [11]. The JP-10 mixtures were heated to 473 K resulting in nozzle exit temperatures $T_o \approx 400$ K which prevented recondensation. The flow control system was similar to that used previously [11] with an uncertainty in the flow rate $< 0.8\%$ for each fluid. Flow rates of JP-10 were metered and vapourised using Bronkhorst Cori-Flow M53 and CEM W-303A units. GC–MS measurements performed on the reactant stream using an Agilent 7890A series GC with a 5975C inert MSD/DS Turbo EI Bundle equipped with 60 m DB-1 column confirmed that no cracking of the fuel had taken place. Coflow velocities were set to 1 m/s in the lower nozzle to prevent overheating and 0.3 m/s in the upper nozzle to remove any large scale bulk motion [11]. Velocity statistics was measured with PIV using a 120 mJ Solo-New

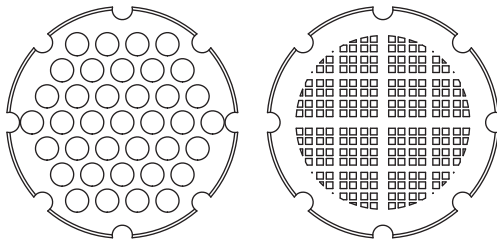


Fig. 2. Left: Grid used to stabilise laminar flames in the lower nozzle. Right: Fractal grid with largest and smallest fractal bar widths of 2.0 mm and 0.5 mm used in the upper nozzle.

Wave Nd:YAG laser with the upper stream seeded with aluminium oxide particles of about 3 μm diameter [11,24] with images processed using decreasing interrogation window sizes from 128×128 via 64×64 to 32×32 with a 50% overlap resulting in velocity vectors spaced about 0.4 mm apart. Laser pulses were separated by 40 μs to minimise spurious vectors.

3. Postprocessing techniques

Velocity statistics were obtained from 1000 images for each case using a purpose written FORTRAN program [24]. A density segregation algorithm [14] was used to detect isocontours marking the instantaneous reaction zone (interface) location. Such methods have been used in the past [14,24–26] and found to be accurate for the detection of conventional flame surfaces with statistical information readily generated. An analysis has been presented by Steinberg et al. [27]. The accuracy of the method in the presence of broadening of the local interface between hot and cold streams was initially evaluated by considering images of the spatial distribution of the mean intensity (\bar{I}_{img}) from all sets of PIV images. The mean intensity in each image was normalised using the mean intensity in a reference window \bar{I}_{win} in the same image where only reactants exist. Particle images have significant deviations in Mie scattering intensities and it was not possible to obtain second order statistics directly. The ability of the algorithm to detect isocontours was first assessed by determining the probability of detecting hot products from the lower nozzle for the limiting case of no added heat release (air emerging from the upper nozzle). The normalised intensity signal $(1 - \bar{I}_{img}/\bar{I}_{win})$ represents the spatial distribution of mean densities relative to that of the unreacted mixtures in the upper stream. Subsequently, the binary images detected by density segregation were binned into windows of 16 pixels (≈ 0.4 mm) wide. The mean values of these images were then calculated for each set to derive the spatial distribution of the mean progress variable (\bar{c})

– directly related to the overall mixing layer (turbulent flame brush) thickness (δ_f). Results obtained using both techniques are shown for all five cases in Fig. 3. No significant discrepancies between the mean spatial distribution of density and the progress variable derived from density segregation are observed.

The PIV images can also be used to estimate the evolution of the interface thickness (δ_f') with a reduction in the Damköhler (Da) number [16]. The centreline profiles of the Mie scattered images were shifted such that the detected iso-contours were located at a datum $x_{shift} = 0$. The shifted profiles were normalised using the corresponding mean image intensity in the reactant stream from the upper nozzle. Profiles with more than one reaction zone were rejected at a rate between 4.5% and 11% depending on the case. The mean reaction zone density can be mapped relative to the detected isocontours and δ_f' was obtained by calculating the mean of the displaced and normalised signal (\bar{I}_{norm}) for every set of 1000 images. Results are shown in Fig. 4 and discussed in Section 4.

The current technique was further evaluated by introducing dry air and methane–air mixtures

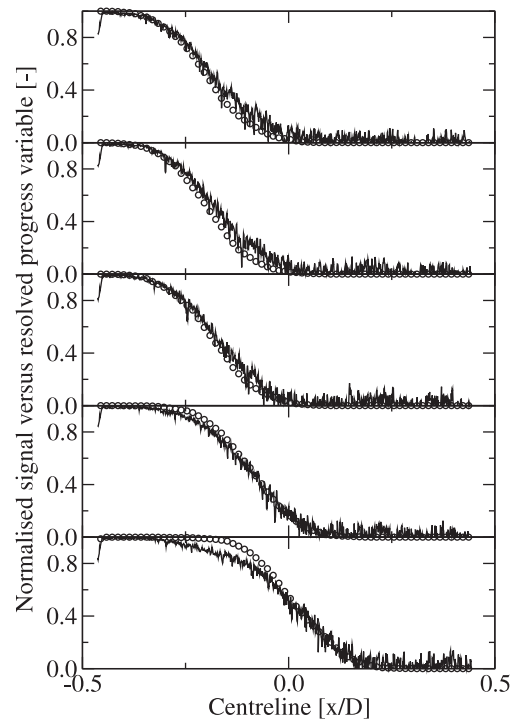


Fig. 3. The impact of interface broadening on \bar{c} obtained using density segregation. Lines: The mean image intensity normalised by the mean image intensity in the reference window $(1 - \bar{I}_{img}/\bar{I}_{win})$. (○) The resolved \bar{c} when aligned with velocity vector locations. Top to bottom: Isothermal case, $\phi = 0.20, 0.40, 0.60$ and 0.80 .

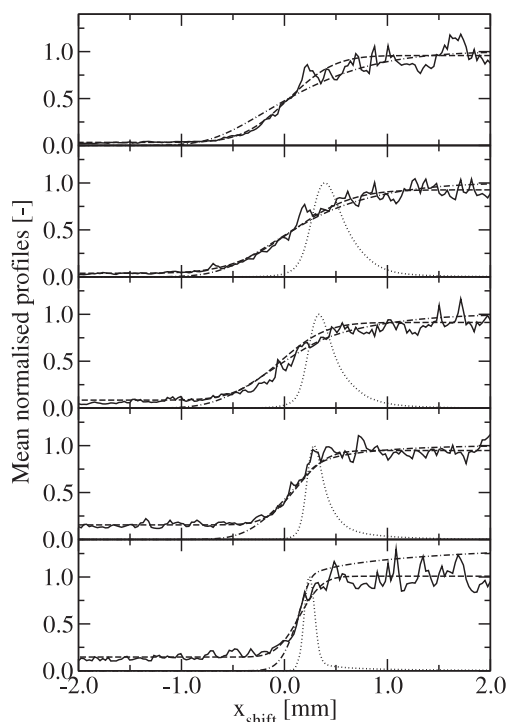


Fig. 4. The evolution of the interface layer (δ_f') thickness. Solid line: Normalised signals \bar{I}_{norm} centred on detected reaction zones. Dashed line: Error function fits. Dot-dashed line: $c = (T - T_o)/(T_b - T_o)$ from a laminar flame solution. Dotted line: The corresponding heat release. Cases as for Fig. 3.

with $\phi = 0.40, 0.60$ and 0.80 at the upper nozzle and performing simultaneous PIV and OH-LIF measurements using a $\text{Ba}(\text{NO}_3)_2$ (barium nitrate) crystal based Raman laser configuration [15] to produce laser light at a wavelength of 281.7 nm. The mean of the OH-LIF images was resolved for each set and subsequently normalised with the mean signals from the exit streams of each nozzle to obtain a reaction progress variable $c = (\bar{I}_{OH} - \bar{I}_{OH,r})/(\bar{I}_{OH,p} - \bar{I}_{OH,r})$, where r and p represent the streams from upper and lower nozzles. The normalised signals from PIV and OH-LIF were compared and an example is shown in Fig. 5. There are no notable differences between the different methods for $\phi \leq 0.6$. The OH-LIF derived profile for $\phi = 0.8$ includes a peak indicating an elevated combustion temperature consistent with the transition to a conventional propagating premixed turbulent flame.

4. Results and discussion

Velocity statistics along the burner radius obtained 2 mm from the upper nozzle exit are pre-

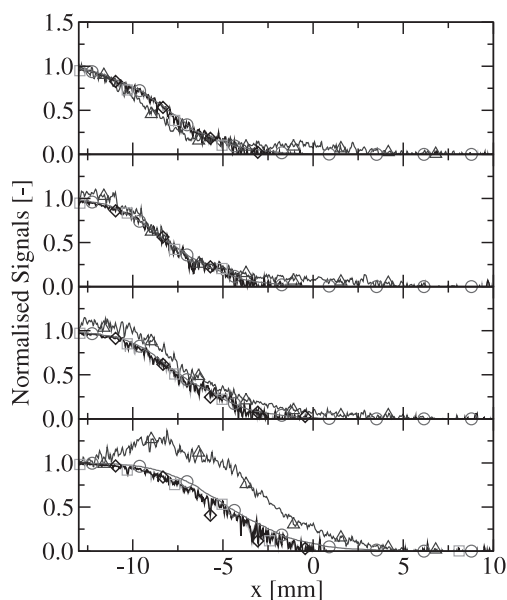


Fig. 5. Application of the density segregation technique and simultaneous PIV and OH-LIF. (□) Mean PIV image intensity normalised by mean image intensity in a reference window $(1 - \bar{I}_{img}/\bar{I}_{win})$. (◇) Mean intensity of normalised PIV images $(1 - \langle \bar{I}_{img,i}/\bar{I}_{win,i} \rangle)$, where i represents the instantaneous image. (Δ) Detected mean progress variable. (Δ) Normalised OH-LIF signals $((\bar{I}_{OH} - \bar{I}_{OH,r})/(\bar{I}_{OH,p} - \bar{I}_{OH,r}))$, where r and p represent reactant streams from the upper and lower nozzles respectively. Top to bottom: Isothermal case, $\phi = 0.40, 0.60$ and 0.80 .

sented in Fig. 6 with the $\phi = 0.20$ and 0.40 data sets omitted due to negligible deviations from the isothermal case. However, significant effects on mean radial velocities were noted for the $\phi = 0.60$ and 0.80 cases. Velocity statistics obtained using conventional PIV along the stagnation point streamline can be found in Fig. 7, where the mean axial velocities (U) and axial (u') and radial (v') rms fluctuations are shown. The data suggests a transitional behaviour with no significant deviations in velocity statistics from the isothermal case until $\phi > 0.4$ and with a clear difference emerging at $\phi = 0.8$. A significant amount of statistics was obtained using the density segregation method. As outlined above, the method is well established for thin reaction zones and can be expected to provide reasonably accurate data in the presence of broadening of the interface layer. The changing nature of the combustion mode is apparent from the progress variable statistics (\bar{c} and \bar{c}') shown in Fig. 8. The mean location of the detected reaction zones in the upper stream show no significant deviations from the isothermal case until $\phi > 0.40$. The result confirms the absence of a propagating turbulent flame. Sample PIV images are shown

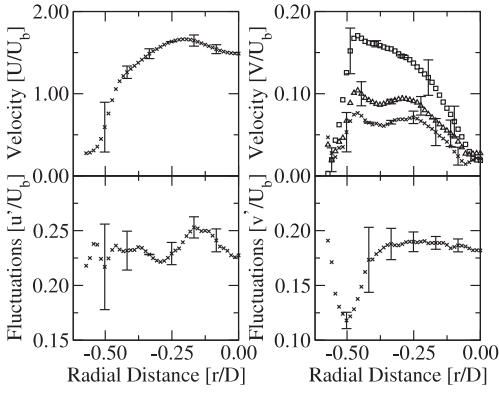


Fig. 6. Normalised mean axial (top left) and radial (top right) velocities along with axial (bottom left) and radial (bottom right) fluctuations measured 2 mm from the burner nozzle exit. Isothermal (\times), $\phi = 0.60$ (Δ) and 0.80 (\square) cases are shown. Data for $\phi = 0.20$ and 0.40 have been omitted as there is no significant deviation from the isothermal case.

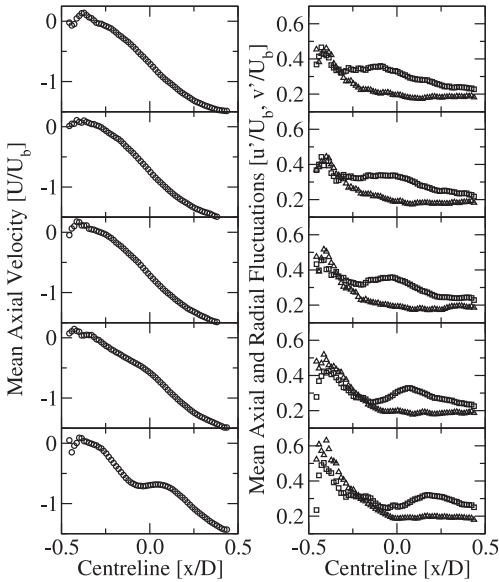


Fig. 7. The mean axial velocity (\circ) (left) and the axial (\square) and radial (Δ) velocity fluctuations (right) along the burner centre axis. Top to bottom: Isothermal case, $\phi = 0.20, 0.40, 0.60$ and 0.80.

in Fig. 9. Pockets of JP-10 combustion products are starting to be observed at $\phi = 0.4$ and indicate the gradual transition to conventional premixed flames as $\phi \rightarrow 0.8$. The temperature of the hot products from the lower nozzle is well above that of auto-ignition and the resulting burning mode for leaner mixtures is related to the HCIDI regime [12] with fuel conversion increasingly sustained by the heat from the combustion products [9,10]. The

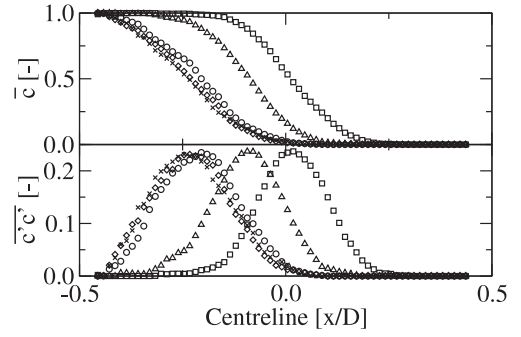


Fig. 8. First (top) and second (bottom) moments of the reaction progress variable (c) along the centre axis of the burner for $\phi = 0.20$ (\diamond), 0.40 (\circ), 0.60 (Δ) and 0.80 (\square), along with (\times) the first (top) and second (bottom) moments of the probability of finding hot products from the lower nozzle with an isothermal stream in the upper nozzle.

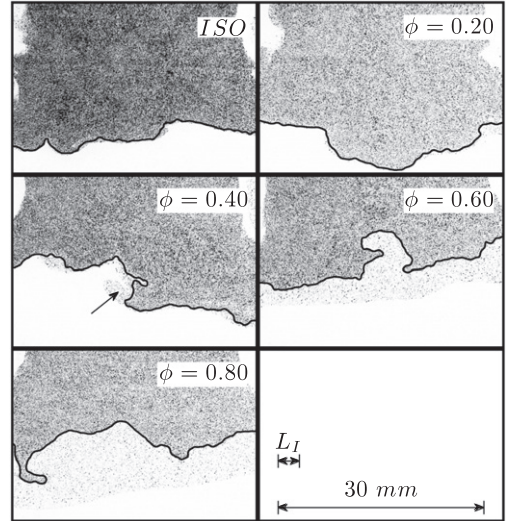


Fig. 9. Examples of PIV images for the different cases with ϕ the equivalence ratio of the JP-10 mixtures in the upper stream. Lines indicate detected reaction zones and the arrow an example of pocket formation. The images are inverted for clarity.

mixing layer thickness (δ_l), defined as the region between the 5th and 95th percentile, was estimated from \bar{c} and the ratio δ_l/L_I remains effectively unchanged with a small increase from 3.2 to 3.5 as ϕ is reduced from 0.6 to 0.4.

Individual images with reaction zones detected via the density segregation technique were further analysed in order to investigate combustion mode transitions. The mean flame lengths in a radial interrogation region of $\pm D/2$ from the centreline were calculated and an integration performed, assuming axial symmetry, on detected reaction

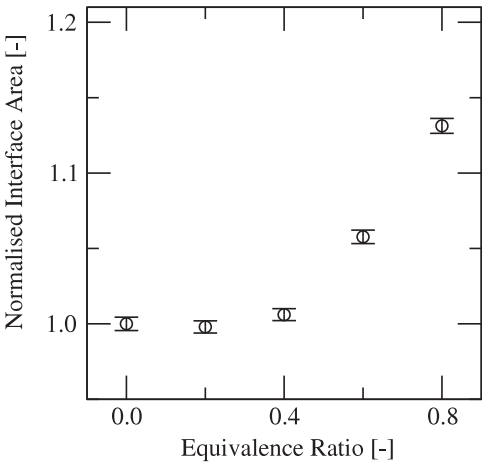


Fig. 10. Statistical analyses of reaction zones from PIV images with the interface area obtained by assuming axial symmetry from $-D/2$ to $D/2$. For $\phi = 0$ the stagnation surfaces were detected and the value used to normalise results.

zones within the width of the nozzle. The normalised results are shown in Fig. 10 and, as suggested above, a distinct transition in the interface (surface) area was found for $\phi \geq 0.4$. Turbulent burning velocities (S_T) were obtained in the manner described by Lawn and Schefer [28] using a mean progress variable (\bar{c}) reference point of 0.02. The resulting values are shown in Table 1. The trend for S_T follows the resolved surface area. The evolution of the 5/95 interface thickness (δ_f^I) with decreasing equivalence ratio was also estimated from the PIV images, as outlined above, with values listed in Table 1.

The laminar flame properties required for comparisons with δ_f^I and the evaluation of the corresponding Da numbers are not readily available

Table 1
Turbulent burning velocities (S_T) of JP-10 and the local axial rms fluctuations (u') at locations where $\bar{c} = 0.02$ [28] along the centre axis of the burner. Damköhler ($Da = (L_I/\delta_f^I)(u_{rms}/S_L)$) numbers [16] based on measured values of $u_{rms} = 0.69$ m/s and $L_I = 3.1$ mm. The laminar flame parameters (δ_f and S_L) were obtained from computations of the corresponding cyclopentadiene flames [33]. The estimated interface thickness (δ_f^I) is also shown.

ϕ	u' [m/s]	S_T [m/s]	δ_f^I [mm]	δ_f [mm]	S_L [m/s]	Da [-]
0.0	1.13	–	1.15	–	–	–
0.2	1.18	2.43	1.57	1.03	0.05	0.23
0.4	1.20	2.56	1.15	0.94	0.06	0.28
0.6	1.14	2.87	0.78	0.76	0.14	0.84
0.8	1.11	3.34	0.58	0.34	0.47	6.0

for JP-10. The relationship of Parsinejad et al. [29] for JP-10 was applied at 400 K to estimate the laminar burning velocity (S_L) at $\phi = 0.80$ resulting in a value of 0.32 m/s. By contrast, laminar flame calculations performed by Courty et al. [30] at 398 K, using the JP-10 chemistry of Li et al. [31], suggest $S_L = 0.51$ m/s at the same stoichiometry. Furthermore, the laminar flame thickness (δ_f) needs to be estimated. Davidson et al. [32] suggested that cyclopentene (C_5H_8) and cyclopentadiene (C_5H_6) are the key breakdown products of JP-10. Accordingly, laminar flame calculations featuring the more reactive C_5H_6 were performed using the chemistry of Robinson and Lindstedt [33] in order to estimate flame parameters at 400 K. The computations featured the experimental geometry and boundary conditions and were well resolved with 400 locally refined control volumes using the standard stagnation flow co-ordinate transformation [34] modified to obtain the rate of strain ($a \simeq 275$ /s) as an eigenvalue. The value of δ_f was determined from the computed 5/95 thickness of the reaction layer based on the heat release. The computed heat release and temperature based reaction progress variable profiles are shown in Fig. 4. The thickness of the reaction layer remains comparatively close to the experiment despite the significant broadening. The corresponding turbulent back-to-back opposed jet flames extinguish at $\phi \sim 0.7$ predominantly due to the impact of turbulent strain. Hence, while a conventional turbulent flame cannot be sustained, combustion remains supported by the hot combustion products in a manner that is consistent with the HC DI regime

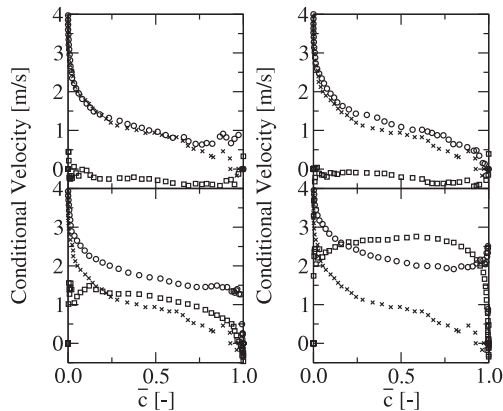


Fig. 11. Axial conditional velocities along the burner axis. (O) reactant (\bar{u}_r) and (□) product (\bar{u}_p) velocities for JP-10 flames. Top left $\phi = 0.20$, top right $\phi = 0.40$, bottom left $\phi = 0.60$ and bottom right $\phi = 0.80$. Reactant (\bar{u}_r) velocities with an isothermal mixture ($\phi = 0$) in the upper nozzle are also shown (x) to highlight the increasing deviation with an increase in the stoichiometry.

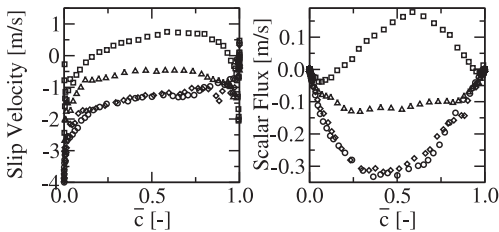


Fig. 12. Mean axial slip velocities \bar{u}_s (left) and scalar fluxes $\bar{u}'c'$ (right) along the burner axis. Equivalence ratios of 0.20 (\diamond), 0.40 (\circ), 0.60 (\triangle) and 0.80 (\square) for lean premixed JP-10 flames.

of flameless oxidation [12]. The relationship to turbulent combustion regimes [16,35] can be explored further. Velocity fluctuations ($u_{rms} = \sqrt{(u'^2 + v'^2)}/3 \approx 0.69$ m/s) in the reactants and the estimated Damköhler numbers are shown in Table 1. The transition from the corrugated flamelet regime to distributed reaction zones is estimated to occur at $\phi \approx 0.8$ and the further transition to the well-stirred regime at $\phi \approx 0.6$. The density segregation technique permits a detailed analysis of conditional statistics of interest to the evaluation of modelling assumptions such as those present in moment [36] and transported PDF [37] based approaches. Mean axial reactant (\bar{u}_r) and product (\bar{u}_p) velocities are shown in Fig. 11 and conditional velocities derived from density segregation can be used to determine slip velocities \bar{u}_s , as defined by Bray [38], and mean scalar fluxes $\bar{u}'c'$ as shown in Fig. 12. Conditional velocities and scalar fluxes show significant deviations from the isothermal case when the equivalence ratio was raised to 0.60 and 0.80. Notably, scalar fluxes show a transition to counter-gradient transport as combustion moves towards the corrugated flamelet regime. The data confirm the continuous transition from a propagating premixed turbulent flame to flameless combustion as the Da number is reduced with the overall structure of the mixing layer increasingly dominated by gradient transport.

5. Conclusions

The continuous transition of lean premixed turbulent JP-10 flames from the corrugated flamelet regime of combustion to a HCDD related regime of flameless combustion has been investigated using an opposed jet geometry with hot combustion products emerging from the lower nozzle. The upper nozzle featured JP-10/air mixtures with equivalence ratios of 0.20, 0.40, 0.60 and 0.80 as well as an isothermal (non-reacting) case ($\phi = 0$) used for comparison purposes. The observed combustion regime transitions were quantified using PIV combined with a density segregation technique for the determination of conditional statis-

tics. The growth in the turbulent burning velocity and flame surface area was also quantified for the more reactive mixtures. In addition to the move to a hot combustion product supported regime of flameless combustion, it was also noted from measured scalar fluxes that turbulent transport changes from a gradient to a counter-gradient mode when moving into the corrugated flamelet regime.

Acknowledgements

The research was carried out with the support of the US Office of Naval Research under grant N00014-07-1-0993. The support of Dr. Gabriel Roy, Dr. Clifford Bedford and Dr. Robert Barlow is gratefully acknowledged. The authors would like to thank Mr. Björn Waldheim for performing the laminar flame calculations and Dr. Frank Beyrau and Mr. Johannes Kerl for sharing the $\text{Ba}(\text{NO}_3)_2$ crystal based Raman laser technique for OH LIF.

References

- [1] F. Weinberg, *Nature* 233 (5317) (1971) 239–241.
- [2] D.R. Hardesty, F.J. Weinberg, *Combust. Sci. Technol.* 8 (5–6) (1973) 201–214.
- [3] M. Katsuki, T. Hasegawa, *Proc. Combust. Inst.* 27 (1998) 3135–3146.
- [4] T. Plessing, N. Peters, J.G. Wünnig, *Proc. Combust. Inst.* 27 (1998) 3197–3204.
- [5] J. Wünnig, J. Wünnig, *Prog. Energy Combust.* 23 (1) (1997) 81–94.
- [6] A. Cavaliere, M. de Joannon, *Prog. Energ. Combust.* 30 (4) (2004) 329–366.
- [7] B.B. Dally, A.N. Karpets, R.S. Barlow, *Proc. Combust. Inst.* 29 (2002) 1147–1154.
- [8] A. Parente, J.C. Sutherland, B.B. Dally, L. Tognotti, P.J. Smith, *Proc. Combust. Inst.* 33 (2011) 3333–3341.
- [9] E. Mastorakos, A. Taylor, J. Whitelaw, *Combust. Flame* 102 (1995) 101–114.
- [10] P. Geipel, K.H.H. Goh, R.P. Lindstedt, The Stability of Flames Burning Against Hot Exhaust Products in Fractal Generated Turbulence, in: Proceedings of the European Combustion Meeting, 2011.
- [11] P. Geipel, K.H.H. Goh, R.P. Lindstedt, *Flow Turbul. Combust.* 85 (2010) 397–419.
- [12] M. de Joannon, A. Matarazzo, P. Sabia, A. Cavaliere, *Proc. Combust. Inst.* 31 (2007) 3409–3416.
- [13] V.D. Milosavljevic, R.P. Lindstedt, M.D. Cornwell, E.J. Gutmark, E.M. Váos, in: G. Roy, K.H. Yu, J.H. Whitelaw, J.J. Witton (Eds.), *Advances in Combustion and Noise Control*, Cranfield University Press, 2005, pp. 149–165. ISBN 1 871315 92 1.
- [14] K.H.H. Goh, P. Geipel, R.P. Lindstedt, Conditional Statistics of Lean Premixed Turbulent Opposed Jet Flames Using Particle Image Velocimetry and Density Segregation, in: Proceedings of the European Combustion Meeting, 2011.

- [15] J. Kerl, T. Sponfeldner, F. Beyrau, *Combust. Flame* 158 (2011) 1905–1907.
- [16] N. Peters, *Turbulent Combustion*, Cambridge Monographs on Mechanics, Cambridge University Press, 2000. ISBN 0 521 66082 3.
- [17] D. Geyer, A. Kempf, A. Dreizler, J. Janicka, *Combust. Flame* 143 (2005) 524–548.
- [18] B. Böhm, C. Heeger, I. Boxx, W. Meier, A. Dreizler, *Proc. Combust. Inst.* 32 (2009) 1647–1654.
- [19] D. Hurst, J.C. Vassilicos, *Phys. Fluids* 19 (2007) 1–31.
- [20] R.E. Seoud, J.C. Vassilicos, *Phys. Fluids* 19 (2007) 1–11.
- [21] J.C. Vassilicos, J.C.R. Hunt, *Proc. Roy. Soc. Lond. A* 435 (1991) 505–534.
- [22] R.P. Lindstedt, K.A. Rizos, *Proc. Combust. Inst.* 29 (2002) 2291–2298.
- [23] T.J. Bruno, M.L. Huber, A. Laesecke, E.W. Lemmon, R.A. Perkins, Thermochemical and Thermophysical Properties of JP-10, NISTIR 6640, National Institute of Standards and Technology, 2006.
- [24] R.P. Lindstedt, D. Luff, J.H. Whitelaw, *Proc. Combust. Inst.* 31 (2007) 1459–1466.
- [25] E. Stevens, K. Bray, B. Lecordier, *Proc. Combust. Inst.* 27 (1998) 949–955.
- [26] S. Pfadler, J. Kerl, F. Beyrau, A. Leipertz, A. Sadiki, J. Scheuerlein, F. Dinkelacker, *Proc. Combust. Inst.* 32 (2009) 1723–1730.
- [27] A.M. Steinberg, J.F. Driscoll, S.L. Ceccio, *Exp. Fluids* 44 (2008) 985–999.
- [28] C. Lawn, R. Schefer, *Combust. Flame* 146 (2006) 180–199.
- [29] F. Parsinejad, C. Arcari, H. Metghalchi, *Combust. Sci. Technol.* 178 (2006) 975–1000.
- [30] L. Courty, K. Chetehoua, F. Halter, V. Bertin, J.P. Garo, C. Mounaïm-Rousselle, On the Emission and Combustion Characteristics of Limonene Involved in Accelerating Forest Fires, in: Seventh Mediterranean Combustion Symposium, 2011.
- [31] S.C. Li, B. Varatharajan, F.A. Williams, *AIAA J.* 39 (2001) 2351–2356.
- [32] D.F. Davidson, D.C. Horning, M.A. Oehlschlaeger, R.K. Hanson, The Decomposition Products of JP-10, in: 37th AIAA/ASME/SAE/ASEE Joint Propulsion Conference and Exhibit, Salt Lake City, 2001.
- [33] R.K. Robinson, R.P. Lindstedt, *Combust. Flame* 158 (2011) 666–686.
- [34] K.M. Leung, R.P. Lindstedt, *Combust. Flame* 102 (1995) 129–160.
- [35] R. Borghi, *On the structure of turbulent premixed flames*, in: C. Bruno, C. Casci (Eds.), *Recent Advances in Aeronautical Science*, Pergamon Press, 1984.
- [36] R.P. Lindstedt, E.M. Váos, *Combust. Flame* 116 (1999) 461–485.
- [37] R.P. Lindstedt, in: K.N.C. Bray, N. Swaminathan (Eds.), *Turbulent Premixed Flames: Physics*, Cambridge University Press, 2011. ISBN 978-0-521-76961-7.
- [38] K.N.C. Bray, *Proc. Roy. Soc. Lond. A* 431 (1990) 315–335.